Universität Karlsruhe (TH)
Institut für Baustatik

On the formulation of geometrically nonlinear3D–Rebar–elements using the enhanced assumed strain method

W. Sprenger, W. Wagner

Mitteilung 1(1997)

Universität Karlsruhe (TH)
Institut für Baustatik

On the formulation of geometrically nonlinear3D–Rebar–elements using the enhanced assumed strain method

W. Sprenger, W. Wagner

Mitteilung 1(1997)

Prof. Dr.–Ing. W. Wagner
Institut für Baustatik
Universität Karlsruhe
Postfach 6980
76128 Karlsruhe

Telefon: (0721) 608–2280
Telefax: (0721) 608–6015
E–mail: bs@.uni-karlsruhe.de
Internet: http://www.bs.uni-karlsruhe.de

On the formulation of geometrically nonlinear 3D–Rebar–elements using the enhanced assumed strain method

W. Sprenger and W. Wagner

Institut für Baustatik, Universität Karlsruhe, Kaiserstr. 12, D-76131 Karlsruhe, Deutschland

This paper presents the combination of the Rebar-concept with the enhanced assumed strain method for geometrically nonlinear 3D-bricks. Finite element calculations with Rebar elements are used to model composite materials with single fibers or fiber layers within one single volume element. The application of global geometric functions to describe single fiber courses, allows an easy computing of single fiber composite structures. In combination with work equivalent nodal forces for the load case prestress, prestressed concrete beams can be calculated. Rebar fiber layer elements are employed successfully for modelling composite laminate structures.

Keywords: finite elements, Rebar element, enhanced assumed strain method, prestressed concrete, composite material

Introduction

Today, structural engineers are able to combine a lot of different materials to new composite materials which contain the desired advantages. The finite element method is generally accepted to investigate the structural and mechanical behaviour of composite materials.
In the seventieth the formulation of Rebar elements has been developed for the modelling of layered structures for tire companies. Such elements are developed and discussed in the last years e.g. from Helnwein et al. [1], Meschke, Helnwein [2], Gebbeken [3] and others. Within 3D–calculations the use of a simple 8 node brick element in comparison to higher order elements may be advantageous due to a rather simple mesh generation and a smaller bandwidth in the solution process. The well known locking effect of such elements in bending situations and for thin shell structures can be reduced substantially using enhanced strains, see e.g. the original work of Simo and Rifai [4].
In this paper we want to combine the strategies of a Rebar formulation with the advantages of the Enhanced Assumed Strain (EAS) method for the geometrically nonlinear 3D case.

The Rebar-concept bases on a combination of different materials within one single element, see e.g. Figure 1. The local position of a fiber(f) and matrix material (m) is described exactly. Thus an accurate and correct mechanical model is derived. The number of degrees of freedom can be reduced because no additional elements have to be introduced for the fibers.

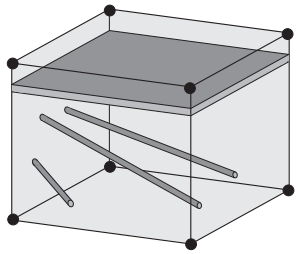

Figure 1: Rebar element

The EAS method bases on a modified definition of the strains [4]:

$$\mathbf{E} := \underbrace{\mathbf{E}^c}_{compatible} + \underbrace{\tilde{\mathbf{E}}}_{enhanced} . \tag{1}$$

$\tilde{\mathbf{E}}$ denotes the 'enhanced' strains in addition to the 'compatible' Green–Lagrange strains $\mathbf{E}^c$. The internal energy is defined with respect to the reference configuration

$$\tilde{\Pi}_i = \int_{V_{tot}} \left[W(\mathbf{E}^c + \tilde{\mathbf{E}}) - \mathbf{S} : \tilde{\mathbf{E}} \right] \, dV \ . \tag{2}$$

Thus the potential becomes a three field functional, depending on the displacements $\mathbf{u}$, the 'enhanced' strains $\tilde{\mathbf{E}}$ and the stresses $\mathbf{S}$

$$\Pi = \Pi(\mathbf{u}, \tilde{\mathbf{E}}, \mathbf{S}) = \tilde{\Pi}_i(\mathbf{u}, \tilde{\mathbf{E}}, \mathbf{S}) + \Pi_a(\mathbf{u}) \ . \tag{3}$$

The paper is organized as follows: first we describe the basic ideas of a combined Rebar–EAS–concept. In the following some examples for single fiber problems are discussed and an example for fiber layers is shown. The paper is closed with a conclusion and an outline.

The EAS-Rebar-Concept

Within the Rebar-concept the internal potential energy is divided in matrix- and fiber material parts

$$\tilde{\Pi}_i = \tilde{\Pi}_{im} + \tilde{\Pi}_{if} \ . \tag{4}$$

At first the total element is described with the material behaviour of the matrix. The volume part associated with the fibers is then corrected. We distinguish between <u>s</u>ingle <u>f</u>ibers and <u>f</u>iber <u>l</u>ayers.

$$\begin{aligned} \tilde{\Pi}_i \ = \ & \int_{V_{tot}} \left[W_m(\mathbf{E}^c + \tilde{\mathbf{E}}) - \mathbf{S}_m : \tilde{\mathbf{E}} \right] \, dV \\ & - \int_{V_{sf}} \left[W_m(\mathbf{E}^c + \tilde{\mathbf{E}}) - \mathbf{S}_m : \tilde{\mathbf{E}} \right] \, dV \ - \int_{V_{fl}} \left[W_m(\mathbf{E}^c + \tilde{\mathbf{E}}) - \mathbf{S}_m : \tilde{\mathbf{E}} \right] \, dV \\ & + \int_{V_{sf}} \left[W_{sf}(\mathbf{E}^c + \tilde{\mathbf{E}}) - \mathbf{S}_{sf} : \tilde{\mathbf{E}} \right] \, dV \ + \int_{V_{fl}} \left[W_{fl}(\mathbf{E}^c + \tilde{\mathbf{E}}) - \mathbf{S}_{fl} : \tilde{\mathbf{E}} \right] \, dV \end{aligned} \tag{5}$$

Basic equations of the EAS-method

Equilibrium holds if the first variation of the potential, see eq. (3), vanishes

$$\delta\Pi = 0 \ . \tag{6}$$

For example we obtain for the first part of eq. (5)

$$\begin{aligned} \delta\tilde{\Pi}^m_{i\,Vtot} \;=\; & \int\limits_{Vtot} \frac{\partial W_m}{\partial \mathbf{E}} : \delta\mathbf{E}^c \; dV \;+\; \int\limits_{Vtot} (\frac{\partial W_m}{\partial \mathbf{E}} - \mathbf{S}_m) : \delta\tilde{\mathbf{E}} \;\; dV \;- \\ & \int\limits_{Vtot} \delta\mathbf{S}_m : \tilde{\mathbf{E}} \; dV \;\; . \end{aligned} \tag{7}$$

The other parts of eq. (5) are calculated in an analogous way.
Furthermore the second variation yields e.g. for the first part of eq. (5)

$$\begin{aligned} \Delta\delta\tilde{\Pi}^m_{i\,Vtot} \;=\; & \int\limits_{Vtot} \left(\delta\mathbf{E}^c \; : \frac{\partial^2 W_m}{\partial\mathbf{E}\partial\mathbf{E}} \; : \Delta\mathbf{E}^c + \frac{\partial W_m}{\partial \mathbf{E}} \; : \delta\Delta\mathbf{E}^c \right) dV + \int\limits_{Vtot} \delta\mathbf{E}^c \; : \frac{\partial^2 W_m}{\partial\mathbf{E}\partial\mathbf{E}} \; : \Delta\tilde{\mathbf{E}} \, dV \\ & + \int\limits_{Vtot} \delta\tilde{\mathbf{E}} \; : \frac{\partial^2 W_m}{\partial\mathbf{E}\partial\mathbf{E}} \; : \Delta\mathbf{E}^c \, dV + \int\limits_{Vtot} \delta\tilde{\mathbf{E}} \; : \frac{\partial^2 W_m}{\partial\mathbf{E}\partial\mathbf{E}} \; : \Delta\tilde{\mathbf{E}} \, dV \\ & - \int\limits_{Vtot} \delta\mathbf{S}_m : \Delta\tilde{\mathbf{E}} \, dV - \int\limits_{Vtot} \delta\tilde{\mathbf{E}} : \Delta\mathbf{S}_m \, dV \, . \end{aligned} \tag{8}$$

Interpolation of the strains and linearization

The isoparametric interpolation of the compatible and the enhanced virtual strains is described by

$$\delta\mathbf{E}^c_{(e)} = \sum_{I=1}^{nodes} \mathbf{B}_I \; \delta\mathbf{v}_I \quad \text{and} \quad \delta\tilde{\mathbf{E}}_{(e)} = \tilde{\mathbf{B}}_E(\xi,\eta,\zeta) \; \delta\boldsymbol{\alpha}_{(e)} \tag{9}$$

with

$$\tilde{\mathbf{B}}_E(\xi,\eta,\zeta) = \frac{det\mathbf{J}_0}{det\mathbf{J}} \; \mathbf{T}_0^{-T} \; \mathbf{M}(\xi,\eta,\zeta) \;\; . \tag{10}$$

$\mathbf{M}$ denotes the 6 x 30 - interpolation matrix, see e.g. Andelfinger, Ramm [5], and $\boldsymbol{\alpha}_{(e)}$ is the vector of the enhanced strain parameters. The Jacobian $\mathbf{J}_0$ and the transformation matrix $\mathbf{T}_0$ are calculated at the center of the isoparametric coordinate system (ξ,η,ζ) , see [6].
Using the orthogonality condition

$$-\int\limits_{V} \delta\mathbf{S} : \tilde{\mathbf{E}} \; dV = 0 \; , \tag{11}$$

which follows from eq.(6), the three field functional reduces to a two field functional. With

$$\mathbb{C} = \frac{\partial^2 W}{\partial\mathbf{E}\partial\mathbf{E}} \qquad \text{and} \qquad \hat{\mathbf{S}} = \frac{\partial \mathrm{W}}{\partial\mathbf{E}} \tag{12}$$

and considering the interpolations for $\delta\mathbf{E}^c$, $\delta\tilde{\mathbf{E}}$ and $\mathbf{N}$ ($\mathbf{u} = \sum\limits_{I=1}^{nodes} \mathbf{N}_I \; \mathbf{v}_I$), we introduce the

following vectors and matrices on element level (e)

$$\begin{aligned}
\mathbf{f}^{int}_{(e)_I} &= \int_V \mathbf{B}_I^T \hat{\mathbf{S}}\, dV \ , & \mathbf{f}^{ext}_{(e)_I} &= \int_V \mathbf{N}_I^T \mathbf{f}\, dV + \int_A \mathbf{N}_I^T \mathbf{t}\, dA \ , \\
\mathbf{K}^{11}_{(e)_{IK}} &= \int_V (\mathbf{B}_I^T \mathbb{C}\, \mathbf{B}_K + \mathbf{G}_{IK})\, dV \ , & \mathbf{K}^{21}_{(e)_I} &= \int_V \tilde{\mathbf{B}}_E^T \mathbb{C}\, \mathbf{B}_I\, dV \ , \\
\mathbf{K}^{12}_{(e)} &= \mathbf{K}^{21^T}_{(e)} \ , & \mathbf{K}^{22}_{(e)} &= \int_V \tilde{\mathbf{B}}_E^T \mathbb{C}\, \tilde{\mathbf{B}}_E\, dV \quad \text{and} \\
\mathbf{h}_{(e)} &= \int_V \tilde{\mathbf{B}}_E^T \hat{\mathbf{S}}\, dV \ . & & \qquad (13)
\end{aligned}$$

Respecting geometrical nonlinearity, the second variation of the internal potential (4) which is needed for the iteration procedure, can be stated as

$$\begin{aligned}
\Delta\delta\tilde{\Pi}_{(e)} &= \sum_{I=1}^{nodes} \delta\mathbf{v}^T_{(e)_I} \left(\sum_{K=1}^{nodes} \mathbf{K}^{11}_{(e)_{IK}} \Delta\mathbf{v}_{(e)_K} + \mathbf{K}^{12}_{(e)_I} \Delta\boldsymbol{\alpha}_{(e)} \right) + \\
&\quad \boldsymbol{\alpha}^T_{(e)} \left(\sum_{K=1}^{nodes} \mathbf{K}^{21}_{(e)_K} \Delta\mathbf{v}_{(e)_K} + \mathbf{K}^{22}_{(e)}\, \Delta\boldsymbol{\alpha}_{(e)} \right) \quad . \qquad (14)
\end{aligned}$$

Thus, the following discrete system of equations with respect to $\Delta\mathbf{v}_{(e)}$ and $\Delta\boldsymbol{\alpha}_{(e)}$ is given on element level

$$\begin{pmatrix} \mathbf{K}^{11}_{(e)} & \mathbf{K}^{12}_{(e)} \\ \mathbf{K}^{21}_{(e)} & \mathbf{K}^{22}_{(e)} \end{pmatrix} \begin{pmatrix} \Delta\mathbf{v}_{(e)} \\ \Delta\boldsymbol{\alpha}_{(e)} \end{pmatrix} = \underbrace{\begin{pmatrix} \mathbf{f}^{ext}_{(e)} - \mathbf{f}^{int}_{(e)} \\ -\mathbf{h}_{(e)} \end{pmatrix}}_{\mathbf{R}_{(e)}} . \qquad (15)$$

The vector of the enhanced strain parameters $\boldsymbol{\alpha}_{(e)}$ can be eliminated on element level

$$\underbrace{(\mathbf{K}^{11}_{(e)} - \mathbf{K}^{12}_{(e)} \mathbf{K}^{22^{-1}}_{(e)} \mathbf{K}^{21}_{(e)})}_{\mathbf{K}_{EAS_{(e)}}} \Delta\mathbf{v}_{(e)} = \underbrace{\mathbf{K}^{12}_{(e)} \mathbf{K}^{22^{-1}}_{(e)} \mathbf{h}_{(e)} + \mathbf{f}^{ext}_{(e)} - \mathbf{f}^{int}_{(e)}}_{\mathbf{R}_{EAS_{(e)}}} , \qquad (16)$$

and the global system

$$\mathbf{K}_{EAS} \Delta\mathbf{v} = \mathbf{R}_{EAS} \qquad (17)$$

remains, which has to be solved, due to the geometrical nonlinearity, with a Newton procedure.

Numerical application of the Rebar-concept

The introduction of the Rebar-concept leads to a further split of terms in eq.(15). For the discretized tangential stiffness matrix of a Rebar element with n_{sf} single fibers and n_{fl} fiber layers it holds on element level

$$\mathbf{K}^{11} = \mathbf{K}^{11}_m - \sum_1^{n_{sf}} \mathbf{K}^{11sf}_m - \sum_1^{n_{fl}} \mathbf{K}^{11fl}_m + \sum_1^{n_{sf}} \mathbf{K}^{11sf}_{sf} + \sum_1^{n_{fl}} \mathbf{K}^{11fl}_{fl} \ . \qquad (18)$$

A_{sf} is the – along the length constant assumed – area of one fiber, h_{fl} is the – over the cross section constant assumed – thickness of the fiber layer defined in the isoparametric space. Thus the different matrices are calculated as

$$\mathbf{K}^{11}_{m_{IK}} = \int_{l_\xi} \int_{l_\eta} \int_{l_\zeta} \left(\mathbf{B}_I^T \mathbb{C}_m \mathbf{B}_K + \mathbf{G}_{IKm} \right) det\mathbf{J}\ d\xi d\eta d\zeta \ , \qquad (19)$$

$$\mathbf{K}^{11sf}_{m_{IK}} = A_{sf} \int_{l_{\xi_{sf}}} \left(\mathbf{B}_I^T \mathbb{C}_m \mathbf{B}_K + \mathbf{G}_{IKm} \right) det\mathbf{J} \; d\xi_{sf} \; , \tag{20}$$

$$\mathbf{K}^{11fl}_{m_{IK}} = h_{fl} \int_{l_{\xi_{fl}}} \int_{l_{\eta_{fl}}} \left(\mathbf{B}_I^T \mathbb{C}_m \mathbf{B}_K + \mathbf{G}_{IKm} \right) det\mathbf{J} \; d\xi_{fl} d\eta_{fl} \; , \tag{21}$$

$$\mathbf{K}^{11sf}_{sf_{IK}} = A_{sf} \int_{l_{\xi_{sf}}} \left(\mathbf{B}_I^T \mathbb{C}_{sf} \mathbf{B}_K + \mathbf{G}_{IKsf} \right) det\mathbf{J} \; d\xi_{sf} \; , \tag{22}$$

$$\mathbf{K}^{11fl}_{fl_{IK}} = h_{fl} \int_{l_{\xi_{fl}}} \int_{l_{\eta_{fl}}} \left(\mathbf{B}_I^T \mathbb{C}_{fl} \mathbf{B}_K + \mathbf{G}_{IKfl} \right) det\mathbf{J} \; d\xi_{fl} d\eta_{fl} \; . \tag{23}$$

$\mathbf{K}^{21}$ and $\mathbf{K}^{22}$ are calculated in an analogous way. The modification of these matrices can be neglected for small fiber parts to reduce the computing time.

$$\mathbf{K}^{21} = \mathbf{K}^{21}_{\mathrm{m}} - \sum_{n=1}^{n_{sf}} \mathbf{K}^{21^{sf}}_{\mathrm{m}} - \sum_{n=1}^{n_{fl}} \mathbf{K}^{21^{fl}}_{\mathrm{m}} + \sum_{n=1}^{n_{sf}} \mathbf{K}^{21^{sf}}_{\mathrm{sf}} + \sum_{n=1}^{n_{fl}} \mathbf{K}^{21^{fl}}_{\mathrm{fl}} \quad \text{and} \tag{24}$$

$$\mathbf{K}^{22} = \mathbf{K}^{22}_{\mathrm{m}} - \sum_{n=1}^{n_{sf}} \mathbf{K}^{22^{sf}}_{\mathrm{m}} - \sum_{n=1}^{n_{fl}} \mathbf{K}^{22^{fl}}_{\mathrm{m}} + \sum_{n=1}^{n_{sf}} \mathbf{K}^{22^{sf}}_{\mathrm{sf}} + \sum_{n=1}^{n_{fl}} \mathbf{K}^{22^{fl}}_{\mathrm{fl}} \; . \tag{25}$$

Fiber orientation

The fiber direction within an element is arbitrary. The material parameter are defined in local directions of the fiber within the matrix $\mathbb{C}_{f,l}$. They have to be transformed with the transformation matrix $\mathbf{T}_\varepsilon$, e.g. [7], to global directions

$$\mathbb{C}_{f,gl} = \mathbf{T}_\varepsilon^T \; \mathbb{C}_{f,l} \; \mathbf{T}_\varepsilon \; . \tag{26}$$

The stress recovery in the fibers is based on

$$\boldsymbol{\sigma}_{\;f,l} = \mathbb{C}_{f,l} \; \mathbf{T}_\varepsilon \; \boldsymbol{\varepsilon}_{\;gl} \; , \tag{27}$$

where $\boldsymbol{\varepsilon}_{\;gl}$ are the global strains in the fiber.

Numerical integration

The different terms in eq. (15) are integrated using standard Gauss–integration (8 points for volume, 4 points for fiber layers and 2 points for single fibers). The necessary geometrical calculations can be found in [7].

General geometric description of single-fiber course

The preparation of the data input is a rather monotonous task when modelling the single fiber with single truss elements. For each truss element the geometrical coordinates have to be calculated. A remarkable simplification is the use of global mathematical functions to describe the exact single fiber course inside the beam. The numbers of all finite elements penetrated by a single fiber and the coordinates of the points of intersection of the tendon with the interfaces of those elements are determined automatically. This procedure leads to a considerable reduction of input data and allows adaptive mesh refinement strategies

or other optimization functions.

Using this general geometrical description of a single-fiber course, it is possible to model prestressed concrete structures. All information of the tendon course are given to compute the loading condition prestress by work equivalent nodal forces (see e.g. Hofstetter and Mang [8] for shells). We transfer this procedure to EAS-Rebar-single-fiber-elements to model prestressed concrete beams.

Method of work equivalent nodal forces

Proposed is the EAS-Rebar-element shown in Figure 2.

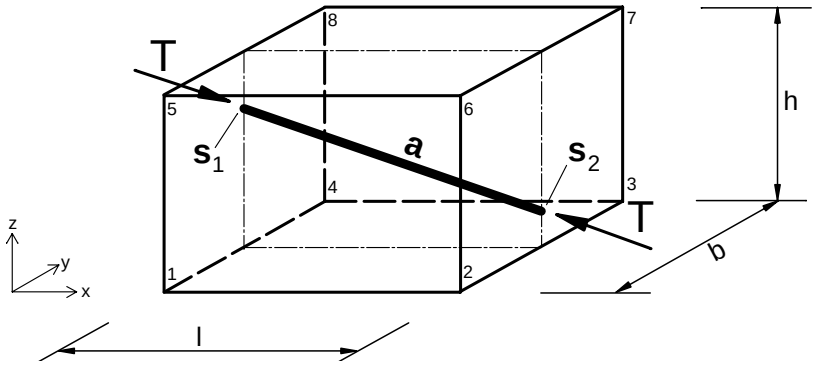

Figure 2: EAS-Rebar-element and tendon force

The tendon force T acts at the points of intersection $\mathbf{s}_1(\xi_{s1}, \eta_{s1}, \zeta_{s1})$ and $\mathbf{s}_2(\xi_{s2}, \eta_{s2}, \zeta_{s2})$. These point loads at the element boundaries replace the forces resulting from curvature of the tendon. The components of the tendon force T are determined with $\mathbf{a} = \mathbf{s}_2 - \mathbf{s}_1$ to

$$T_i = \frac{1}{\|\mathbf{a}\|}\, a_i\, T \quad \text{with} \quad i = x, y, z \quad . \tag{28}$$

When calculating the tendon force, a constant distribution of the tendon force is assumed as a simplification. Prestress losses during the tensioning operation, as example friction between the tendon and the duct or slip of the tendon in the anchorage, can easily be integrated, see e.g. [9]. These problems are not taken into account here.

The work equivalent nodal forces (28) are, depending on the position of the tendon in the element, distributed over the nodes I of the element

$$T_I = N_I(\xi_{sj}, \eta_{sj}, \zeta_{sj})\; T \quad \text{with } I = 1, 2, .., 8 \text{ and } j = 1, 2 \; . \tag{29}$$

Work equivalent nodal forces can also be discussed as a supplement Π_a^T of the external potential which leads to the following additional term:

$$\mathbf{f}_{(e)_I}^{ext} = \int_V \mathbf{N}_I^T \mathbf{T}\; dV \; . \tag{30}$$

Numerical studies with EAS-Rebar-single-fiber-elements

The efficiency of the new EAS-Rebar-element, which has been implemented in an enhanced version of the program **FEAP**, documented in Zienkiewicz and Taylor [10], is demonstrated by some examples. Prestressed concrete structures are modelled with EAS-Rebar-single-fiber-elements.
When assuming full composite action without friction losses between tendon and concrete, the ideal values of the cross section have been used for the analytical calculation of the stresses.
Taking statical determination and elastic material response without formation of cracks in concrete as a basis, the stress in the concrete under prestress, is calculated with

$$\sigma_{b,v} = -\frac{T}{A_i} - \frac{T\, z_{iz}}{I_i}\, z_i \quad (a) \qquad \text{or} \quad \sigma_{b,v} = -\frac{T}{A_i} - \frac{M}{W_i} \quad (b) \quad . \tag{31}$$

In contrast to the formulation of equation (31a) the moment M in equation (31b) is determined via an uniform longitudinal loading condition and forces as well as moments acting at the ends of the beam. These deviation forces approximate the loading condition of prestress.

The tendon-stress is determined via the concrete stress $\sigma_{bz,v}$ at the position of the tendon with

$$\sigma_{z,v} = \sigma_{z,v}^{(0)} + n\, \sigma_{bz,v} = \frac{T^{(0)}}{A_z} + n\, \sigma_{bz,v}\, . \tag{32}$$

Simple beam with parabolic cable profile and rectangular cross section

Here a beam under prestress $T = 1\ MN$ is discussed.

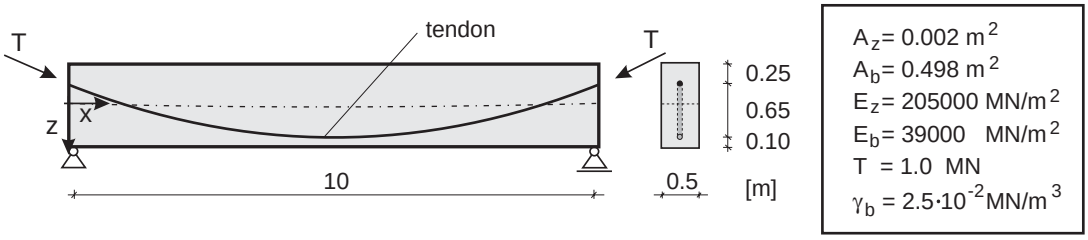

Figure 3: Simple beam with parabolic cable profile

The beam cross section is modelled with two elements, see Fig. 3.

FE-Calculation of the loading condition prestress with deviation forces in comparison to work equivalent nodal forces

Often, even in FE-calculations, the loading condition of prestress is modelled by the method of deviation forces (mdf), which is as well known as load balancing concept [11]. In Figure 4 this method is compared to the method with work equivalent nodal forces and also to an analytical calculation as shown in (31a). Figure 4 shows results for the normal stress at the lower edge in the middle of the beam.

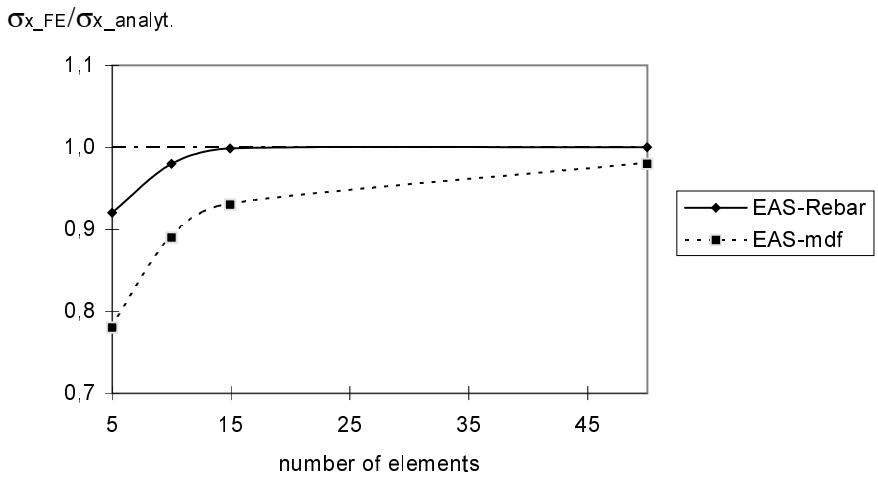

Figure 4: Comparison of FE-Calculation: EAS-mdf to EAS-Rebar

Using EAS-Rebar elements leads to much better results than the usual EAS-method with deviation forces when monitoring the convergence of the respective curve.

FE-Calculation with EAS-Rebar-elements in comparison to simple Rebar elements for the loading condition of prestress

In the following we compare FE calculations using Rebar elements (without EAS-method) and EAS-Rebar-elements with analytical calculations.

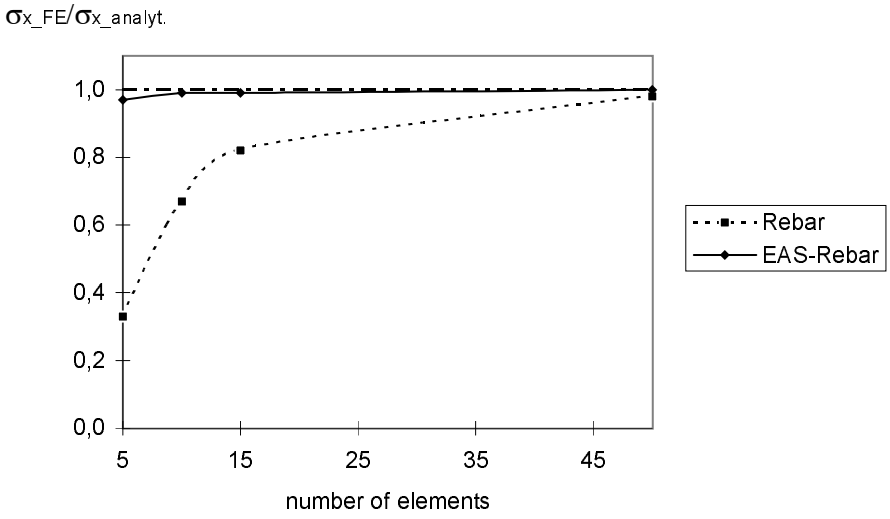

Figure 5: Convergence of the Rebar and the EAS-Rebar-element

Figure 5 shows normal stresses σ_x at the lower edge, in the middle of the beam depending on the number of elements per length and the method employed.
Even combined with Rebar elements the EAS-method reduces the locking-effect in a drastic way.

Prestressed two field beam with T-cross-section

One typical application for prestressed structures is a T-beam.

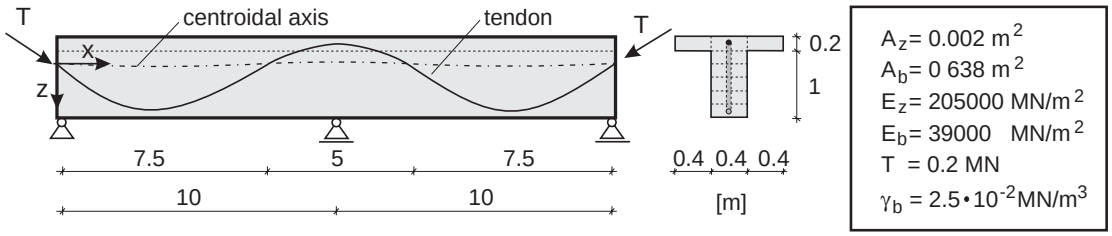

Figure 6: Prestressed two field beam

The parabolic tendon course extends over three zones. The tendon intersects at all zone limits with the centroid of the T-beam at the height $z = 0.725\ m$. A reference analysis has been carried out through the method with deviation forces (equation (31b)).
The beam is modelled with 60 elements over the length. The discretization of the cross section can be seen in Figure 6. The FE-calculations have been performed with the conventional mdf-method as well as with the Rebar and the new EAS-Rebar-element.
The generation of the input data when using Rebar or EAS-Rebar-elements is restricted on the additional input of the tendon course in form of a mathematical function and the material data. The mdf-method requires either a cumbersome preparation of the input or a complicated pre-processor-program. In the case of a possible adaptive mesh refinement this laborious input generation has to be repeated and may lead to a considerable change of the original input data. On the other hand it is very simple to optimize the course of the tendon using Rebar or EAS-Rebar-elements.

The results are compared in Figure 7. Here the normal stress distribution along x at the top of the beam is shown.

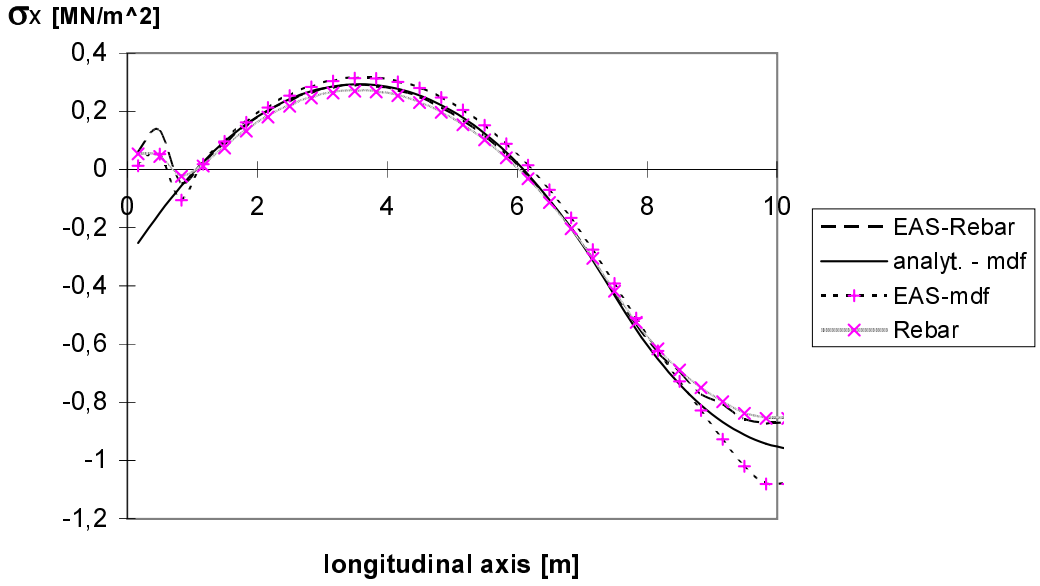

Figure 7: Normal stress distribution along x at top of the beam

The stresses, determined with Rebar, EAS-Rebar-elements and the method of deviation forces, correspond well with the analytical reference values in zones where the beam theory is valid. Differences occur only in bearing- and force admitting-areas.

Prestressed two-bay-beam with rectangular cross-section

One typical kind of failure is buckling of a beam with a slender cross section. System and cross section are shown in Figure 8.

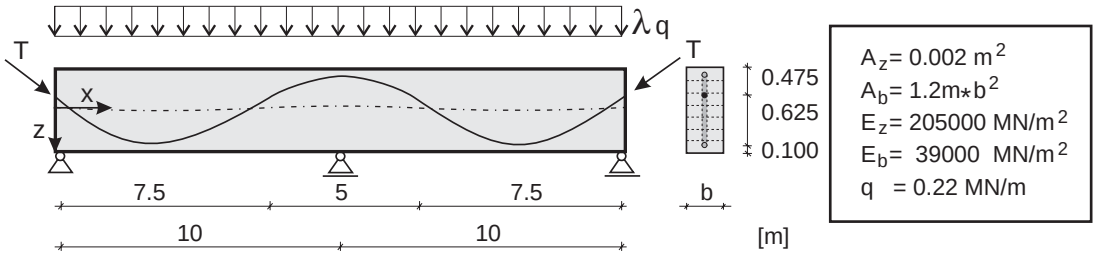

Figure 8: Prestressed two-bay-beam with rectangular cross-section

The beam has a trunnion bearing at each bearing area. The imposed load q grows proportional to the load factor λ. Figure 9 shows the buckling load factor with respect to the tendon force T for three different cross sections with various width.

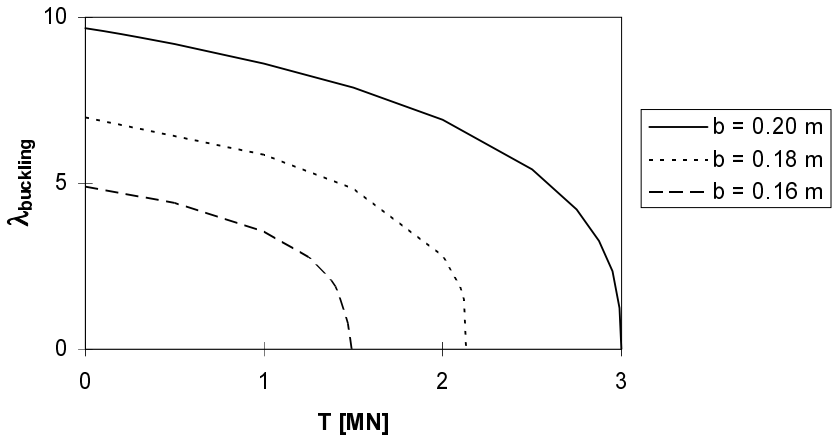

Figure 9: Buckling load factors as a function of the prestress and the width of the cross-section

The buckling load decreases when the tendon force is increased. Under pure prestress the maximum tendon force T is equal to the Euler buckling load. An increase in the width of the cross section leads to an increase of the buckling load. Figure 10 shows the first eigenvector of the prestressed beam with $b = 0.16m$ at the buckling load factor $\lambda_{buckling}$.

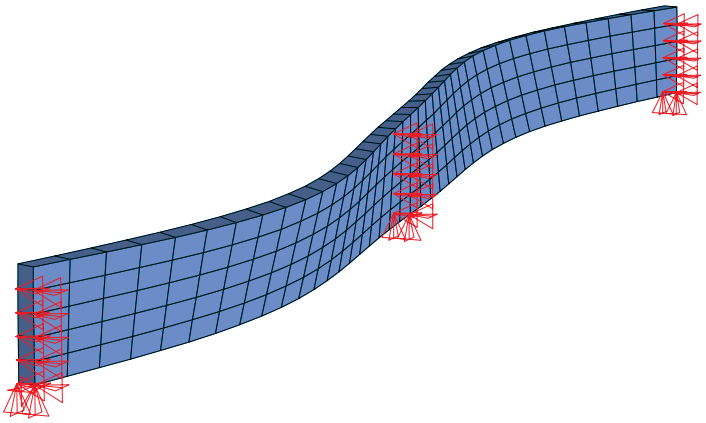

Figure 10: First eigenvector for $\lambda = \lambda_{buckling}$

Numerical study with EAS-Rebar-fiber-layer-elements

Buckling of a sandwich plate

Next, the buckling load of the sandwich plate is calculated, see for comparison Starlinger [12].

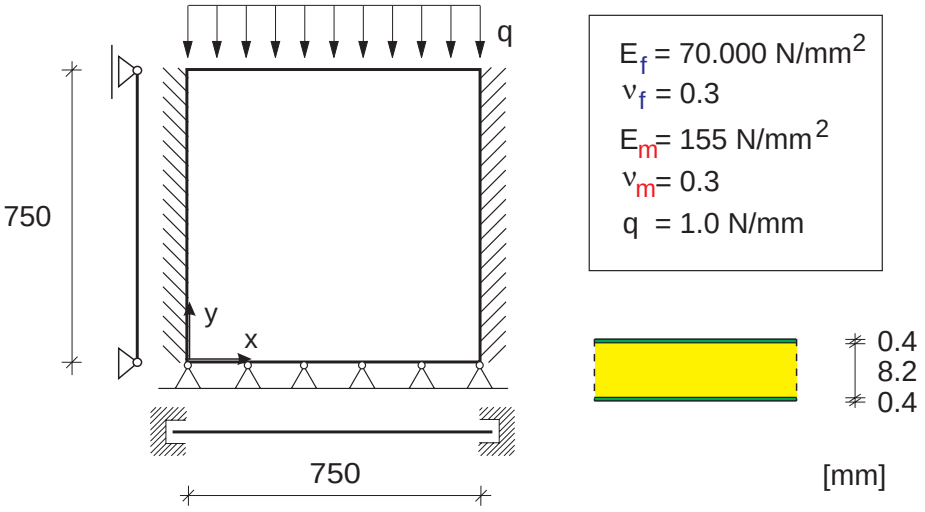

Figure 11: Sandwich plate: geometry and material

System and material data as well as the assumed boundary conditions are shown in Figure 11. The two aluminium layers are calculated each with one fiber-layer and two Gauss points through the layer-thickness. According to Pflüger [13] the critical global buckling load can be determined analytically.

To model the Navier boundary conditions with 3D elements at $y = 0$ mm at the midplane of the plate two possibilities exist, see Figure 12.

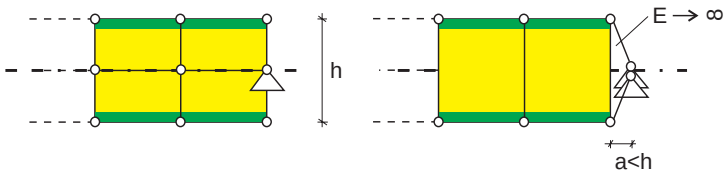

Figure 12: Modelling of Navier boundary conditions

Results are depicted in table 1 for different types of calculation. A very good agreement between the analytical solution, the solution of Starlinger, based on finite shell elements and the solutions based on EAS-Rebar-elements can be seen. Even with one element over the thickness an accurate description of the problem is possible with EAS-Rebar-elements.

Ref.	Mesh	Buckling load [N/mm]
Pflüger	analytically	119.8
Starlinger	15x15x1	101.1
EAS-Rebar	10x10x2	119.6
EAS-Rebar	15x15x1	115.8

Table 1: Buckling loads for sandwich plate

Summary and outlook

In this paper the theoretical and numerical foundations of a new EAS-Rebar-element on the basis of the standard 3D-brick element have been discussed. The EAS-method has been integrated into the Rebar element successfully. The locking behaviour of the 3D element has been eliminated to a large extend.

EAS-Rebar-single-fiber-elements are suitable for modelling composite laminates, in which only few single (numerical or real) fibers occur.
One field of application is the modelling of prestressed concrete structures. In this paper the essential advantages using EAS-Rebar-single-fiber-elements in contrast to the conventional method with deviation forces has been demonstrated by examples.
The introduction of work equivalent nodal forces allows the accurate description of the loading condition of prestress with EAS-Rebar-elements.

EAS-Rebar-fiber-layer-elements are used in modelling coursed materials. For example smeared layer structures (e.g. reinforcement layers in concrete) or real laminate structures (e.g. fiber composite laminate) can be examined. The various number of integration points along the width of the fiber-layer, depending on the proportion of the volume from the fiber-material compared with the total volume, has to be observed.

Acknowledgments

The financial support of the Deutsche Forschungsgemeinschaft (DFG) is gratefully acknowledged. The authors thank their coworker S. Klinkel for helpful discussions.

List of notations in alphabetical order

$\boldsymbol{\alpha}$:	vector of enhanced strain parameters	A_b:	concrete cross section
A_i:	idealized cross section	A_{sf}:	area of one single fiber in isoparametric space
A_z:	cross section of tendon	$\mathbf{B}_I$:	matrix with derivations of shape functions
$\mathbb{C}_f$:	material matrix of fiber material	$\mathbb{C}_{fl}$:	material matrix of fiber layer
$\mathbb{C}_{f,l}$:	material matrix of fiber material in local coordinate system	$\mathbb{C}_{f,gl}$:	material matrix of fiber material in global coordinate system
$\mathbb{C}_m$:	material matrix of matrix material	$\mathbb{C}_{sf}$:	material matrix of single fiber
$\mathbf{E}$:	strain tensor	E_b:	Young's modulus of concrete
$\mathbf{E}^c$:	Green-Lagrange-strain tensor	E_f:	Young's modulus of aluminium
E_m:	Young's modulus of matrix material	E_z:	Young's modulus of steel
$\tilde{\mathbf{E}}$:	enhanced strain tensor	$\mathbf{f}$:	volume load
γ_b:	specific gravity of concrete	$\mathbf{G}_{IK}$:	initial stress matrix
h_{fl}:	thickness of one fiber layer in isoparametric space	I_i:	idealized moment of inertia
$\mathbf{J}$:	Jacobian matrix	$\mathbf{J}_0$:	Jacobian matrix at the center of the element
$\mathbf{M}$:	interpolation matrix for enhanced strains	n:	reduction factor
$\mathbf{N}$:	matrix of shape functions	n_{fl}:	number of fiber layers
n_{sf}:	number of single fibers	ν_f:	Poisson's ratio of aluminium
ν_m:	Poisson's ratio of matrix material	Π_a:	external potential
Π_i:	internal potential	q:	applied load
$\mathbf{S}$:	stress tensor	$\mathbf{S}_{fl}$:	stress tensor of fiber layer
$\mathbf{S}_m$:	stress tensor of matrix material	$\mathbf{S}_{sf}$:	stress tensor of single fiber
$\sigma_{bz,v}$:	stress in concrete owing prestress on position of tendon	$\sigma_{f,l}$:	fiber stress in local direction
$\sigma_{z,v}$:	stress in tendon owing prestress	$\sigma^{(0)}_{z,v}$:	stress in tendon owing prestress without prestress losses
$\mathbf{t}$:	surface load	T:	tendon force
$T^{(0)}$:	tendon force without prestress losses	$\mathbf{T}_0$:	transformation matrix for enhanced strains at the center of the element
$\mathbf{T}_\varepsilon$:	transformation matrix for strains	$\mathbf{u}$:	displacement vector
V_{fl}:	volume of fiber layer	$\mathbf{v}_I$:	nodal displacement vector
V_{sf}:	volume of single fiber	V_{tot}:	total element volume
W_{fl}:	strain energy density of fiber layer	W_i:	idealized section modulus
W_m:	strain energy density of matrix-material	W_{sf}:	strain energy density of single fiber
ξ, η, ζ:	isoparametric coordinates	z_i:	z-coordinate of idealized cross section
z_{iz}:	z-coordinate of tendon on idealized coordinate system		

References

[1] Helnwein, P.; Liu, C.H.; Meschke, G.; Mang, H.A.: A new 3-D finite element model for cord-reinforced rubber composites – Aplication to analysis of automobile tires, Finite Elements in Analysis and Design 14, 1993, 1-16

[2] Meschke, G.; Helnwein, P.: Large-strain 3d-analysis of fibre-reinforced composites using rebar elements: hyperelastic formulations for cords, Comp. Mech. 13, 1994, 241-254

[3] Gebbeken, N.: Zur Untersuchung des linearen Tragverhaltens von Faserverbundkonstruktionen mittels numerischer Methoden, Report No. 96/1, Universität der Bundeswehr München, 1996

[4] Simo, J.C.; Rifai, D.: A Class Of Mixed Assumed Strain Methods And The Method Of Incompatible Modes, Int. J. Num. Meth. Eng. 29, 1990, 1595-1638

[5] Andelfinger, U.; Ramm, E.: EAS-Elements for Two-Dimensional, Threedimensional Plate and Shell Structures and their Equivalence to HR-Elements, Int. J. Num. Meth. Eng. 36, 1993, 1311-1337

[6] Klinkel, S.; Wagner, W.: A Geometrical Nonlinear Brick Element based on the EAS-Method, accepted for publication in Int. J. Num. Meth. Eng.

[7] Sprenger, W.; Theorie und Finite-Elemente-Entwicklung eines geometrisch nichtlinearen, 3 dimensionalen Rebar-Elementes, Diploma-Thesis, Institut für Baustatik, Karlsruhe, 1996

[8] Hofstetter, G; Mang, H.A.: Work-equivalent node forces from prestress of concrete shells, Finite element methods for plate and shell structures, formulations and algorithms, (Eds. T. J. R. Hughes and E. Hinton) Pineridge Press, Swansea, Vol. 2, 1986, 312-347

[9] Hofstetter, G.: Physikalisch und geometrisch nichtlineare Traglastanalysen von Spannbetonscheiben, -platten und -schalen mittels der Methode der finiten Elemente, Dissertation, TU Wien, 1987

[10] Zienkiewicz, O.C.; Taylor, R. L.: The Finite Element Method, Vol. I+II, 4th edn, McGraw-Hill, London, 1989/1991

[11] Leonhardt, F.: Vorlesungen über Massivbau - Fünfter Teil: Spannbeton, Springer-Verlag, Berlin, 1980

[12] Starlinger, A.: Development of Efficient Finite Shell Elements for the Analysis of Sandwich Structures und Large Deformations and Global as well as Local Instabilities, VDI-Verlag, Reihe 18, Nr. 93, Düsseldorf, 1991

[13] Pflüger, A.: Stabilitätsprobleme in der Elastostatik, Springer-Verlag, Berlin, 1975